The effect of gamma radiation on the mechanical and microstructural properties of Fe-rich inorganic polymers

Peer-reviewed author version

MAST, Bram; Gerardy, Isabelle; Pontikes, Yiannis; SCHROEYERS, Wouter; RENIERS, Brigitte; SAMYN, Pieter; Gryglewicz, Grazyna; VANDOREN, Bram & SCHREURS, Sonja (2019) The effect of gamma radiation on the mechanical and microstructural properties of Fe-rich inorganic polymers. In: Journal of nuclear materials = Journal des matériaux nucléaires, 521, p. 126-136.

DOI: 10.1016/j.jnucmat.2019.04.045
Handle: http://hdl.handle.net/1942/28255

Accepted Manuscript

The effect of gamma radiation on the mechanical and microstructural properties of Fe-rich inorganic polymers

Bram Mast, Isabelle Gerardy, Yiannis Pontikes, Wouter Schroeyers, Brigitte Reniers, Pieter Samyn, Grazyna Gryglewicz, Bram Vandoren, Sonja Schreurs

PII: S0022-3115(19)30020-0

DOI: https://doi.org/10.1016/j.jnucmat.2019.04.045

Reference: NUMA 51593

To appear in: *Journal of Nuclear Materials*

Received Date: 7 January 2019

Revised Date: 1 April 2019

Accepted Date: 28 April 2019

Please cite this article as: B. Mast, I. Gerardy, Y. Pontikes, W. Schroeyers, B. Reniers, P. Samyn, G. Gryglewicz, B. Vandoren, S. Schreurs, The effect of gamma radiation on the mechanical and microstructural properties of Fe-rich inorganic polymers, *Journal of Nuclear Materials* (2019), doi: https://doi.org/10.1016/j.jnucmat.2019.04.045.

The effect of gamma radiation on the mechanical and microstructural properties of Fe-rich inorganic polymers

Bram Mast[a*], Isabelle Gerardy[b], Yiannis Pontikes[c], Wouter Schroeyers[a], Brigitte Reniers[a], Pieter Samyn[d], Grazyna Gryglewicz[e], Bram Vandoren[f], Sonja Schreurs[a**]

[a] Hasselt University, CMK, NuTeC, Nuclear Technology - Faculty of Engineering Technology, Agoralaan Building H, B-3590 Diepenbeek, Belgium

[b] Haute Ecole Bruxelles-Brabant HE2B, ISIB, Engineering Education Institute, Physical and Nuclear Department, Koningsstraat 150, B-1000 Brussels, Belgium

[c] KU Leuven, Department of Materials Engineering, Kasteelpark Arenberg 44, 3001 Heverlee, Belgium

[d] Hasselt University, Research Group of Applied and Analytical Chemistry, Agoralaan Building D, B-3590 Diepenbeek, Belgium

[e] Wrocław University of Science and Technology, Faculty of Chemistry, Department of Polymer and Carbonaceous Materials, Gdańska 7/9, 50-344 Wrocław, Poland

[f] Hasselt University, CERG, Faculty of Engineering Technology, Agoralaan Building H, B-3590 Diepenbeek, Belgium

[*] Main Author, E-mail: bram.mast@uhasselt.be

[**]Corresponding Author: sonja.schreurs@uhasselt.be

Keywords:

Alkali Activated Materials, Fe-rich inorganic polymers, gamma irradiation, mechanical and microstructural changes,

Declarations of interest: none

Abstract

Inorganic Polymers (IPs) are interesting alternative binder materials to Ordinary Portland Cement (OPC). They could be potentially used in applications such as nuclear safety structures and radioactive waste management since they are highly chemically and thermally resistant. However, their chemical and mechanical stability still has to be proven when irradiated at the very early age.

This study investigated the effect of gamma irradiation on the mechanical and microstructural properties of IPs cured for 1 hour, 24 hours or 28 days. For that purpose, IPs were irradiated using different dose rates (1.6 Gy/h, 7.1 Gy/h, 152 Gy/h and 2 kGy/h) until different absorbed doses with a maximum of 624 kGy. The effects were evaluated by means of compressive strength tests, microstructural analysis by image analysis, porosity analysis (water absorption and MIP), thermogravimetric analysis (TGA) and infrared spectrometry. For each irradiation test, non-irradiated samples were kept as a reference at the same environmental conditions as the irradiated samples. The results were compared with similar studies on OPC-based samples.

At low doses (< 5 kGy) no statistically significant change has been found. Above 5 kGy however, a significant increase in compressive strength was found for all the samples tested. An increase up to 22 % in compressive strength was observed for the samples irradiated at 2 kGy/h. Gamma radiation induced carbonation, Fe^{3+} reduction and polymerization could explain the strength increase but need further investigation.

Graphical Abstract

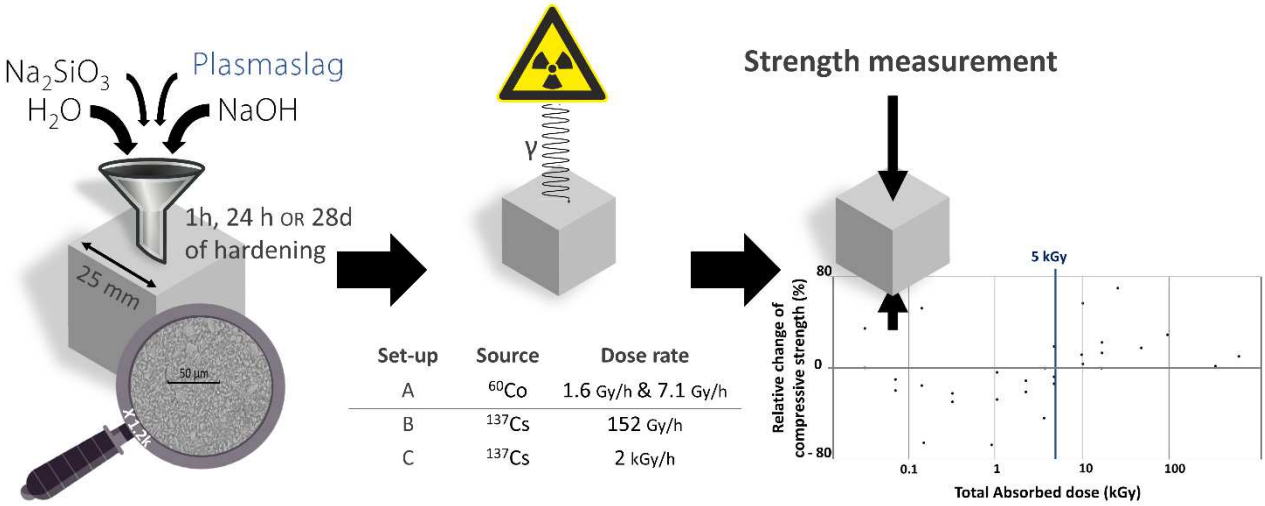

Highlights

- Plasma slag-based IPs were irradiated using gamma sources.
- Below 5 kGy no significant changes were observed
- Above 5 kGy an increase of compressive strength was observed.
- The total absorbed dose is of higher importance than the applied dose rate.
- The curing time before gamma irradiation influences the material its response.

Abbreviations:

IPs	*Inorganic Polymers*
OPC	*Ordinary Portand Cement*
SEM	*Scanning Electron Microscope*
MIP	*Mercury Intrusion Porosimetry*
TGA	*Thermogravimetrical Analysis*
ATR-FTIR	*Attenuated Total Reflection Fourier-transform Infrared Spectroscopy*
PS	*Plasma Slag*
BET	*Brunauer–Emmett–Teller*
WA	*Water Absorption*

1 Introduction

For some decades, alternatives for cementitious barriers for shielding and radioactive waste encapsulation have been studied worldwide. Calcium(alumino)silicate cements are currently used to condition low and intermediate level radioactive nuclear waste [1]. These materials have a good mechanical strength and chemical stability. However, alternatives to the commonly used ordinary Portland cement (OPC) matrices are increasingly being studied to enhance the very long term durability [2].

Inorganic Polymers (IPs) are one of the alternatives currently being studied intensively. IPs are a class of inorganic binders which can be formed through the alkali activation of an aluminosilicate or ferrosilicate precursor, e.g. fly ash and granulated blast furnace slag. A three-dimensional-tetrahedral network is formed in which the aluminates and silicates are covalently bonded by shared oxygen atoms [3]. Alkali activation technology has been recognized to offer high potential for immobilization of hazardous components [4]. The high pH of the materials insolubilizes many metals and radioelements such as ^{137}Cs and protects metals from corrosion effects [5], [6], [7]. Additionally, these binders have promising properties as high chemical and temperature resistance [3], [8], making them interesting candidates for application in nuclear safety structures. In 2013, the first IP was introduced successfully for nuclear waste encapsulation. SIAL® [9] was developed and used to immobilise a highly contaminated sludge for which conventional methods using cementation or bitumen treatment could not be used due to the presence of radionuclides, including ^{137}Cs. This material can incorporate four times as much waste as a traditional cement matrix and the encapsulation process takes less time. The material has a higher mechanical strength, lower leachability for radionuclides, low fire risk, high radiation stability and good physical stability in the presence of frost and water [9], [10]. However, a decrease in compressive strength ranging from 16 to 39 % was found when this material was irradiated to a total dose of 1.027 MGy using a ^{60}Co source with a dose rate of 2.5 kGy/h [10].

In 2013, the International Atomic Energy Agency (IAEA) [2] pronounced its interest in four types of alternative cementitious materials for use in nuclear safety structures, including geopolymers, magnesium phosphate cements, calcium aluminate cements and calcium sulfoaluminate cements [11], [12]. The use of geopolymer-type materials however still requires precursor standardization and process optimization. Moreover, understanding the durability of IPs is a fundamental prerequisite before they can be used in nuclear applications.

Several studies have already proven the detrimental effect of gamma radiation on OPC-based matrices, due to changes in compressive strength, changes in average pore diameter, radiation induced carbonation and the formation of microcracks [13]–[20]. However, only a few studies examining the effect of gamma radiation on IPs are published [5], [21], [22].

A decrease in compressive strength for hardened concrete with a total absorbed gamma dose above 10^8 Gy was mentioned by Hilsdorf et al. in 1978 [13]. According to Ichikawa and Koizumi [14] gamma rays only affect the characteristics of the hardened concrete for doses higher than 10^{10} Gy. Soo and Milian [15] and Vodák et al. [16] found that the compressive strength drops with 10 to 15% once the dose exceeds about 10^5 Gy due to radiolysis of the water in the pores and hydrates (reaction products) of the OPC matrices. The latter might cause shrinkage of the cement paste and the formation of microcracks and thereby increase the average pore diameter. Rosseel et al. [17] and Kontani et al. [18] however concluded that only a small percentage (1%) of the chemically bonded water will decompose, even when subjected to a dose close to the reference level of 10^8 Gy. Additionally, when radiolysis is taking place, hydrogen peroxide H_2O_2 will be formed which can react with cement calcium (from cement hydration) to form insoluble calcium peroxide, $CaO_2.8H_2O$. The dehydrated peroxide reacts with water to form portlandite $Ca(OH)_2$ which in turn can react with CO_2 to form $CaCO_3$ [23]. It is confirmed by the experiments of Maruyama et al. (2018), who irradiated fully hydrated OPC mortars up to 5 x 10^4 kGy at ± 7 kGy/h, that aragonite and vaterite are preferentially formed under irradiation while mainly calcite was formed without gamma radiation [24]. Also a decrease in average pore diameter can be observed [16]. It was found that under irradiation vaterite, which is less dense then calcite, can fill the small pores around C-S-H [24]. Changes in pore size distribution are thus dependent on two competing processes: carbonation and radiolytic dehydration [16]. According to Maruyama et al. [24], radiation-altered carbonation could increase the strength of the Portland cement paste due to pore filling and the formation of pseudomorph C-S-H. On the other hand, the formation of calcite may contribute to the formation of microcracks and give rise to an increased porosity[17]. Łowińska-Kluge and Piszora [19]

reported a modification of the cement composites' morphology due to gamma radiation from amorphization of cement hydrates. Mainly covalent bonds of e.g. Si-O are thought to be sensitive for gamma irradiation due to the electronic excitations cause when a gamma ray interacts with matter [25]. Hilloulin et al. [20] mentioned an increase of the cement paste creep modulus and harness and decrease of the creep characteristic time for a gamma irradiation up to 257 kGy at 8.5 Gy/h. The samples used in the previously mentioned studies had already a certain state of hardening prior to irradiation which is not the case for all barrier systems used in nuclear waste encapsulation.

In most gamma irradiation experiments, no distinction is made between damage caused by gamma-ray heating and damage caused by the radiation itself since they cannot be uncoupled. According to Maruyama et al. [24], a temperature increase is expected for the sample of more than 5 °C at the sample surface for an irradiation at ± 7 kGy/h. This, together with the radiolysis of water, leads to an accelerated drying of the material which also influences the carbonation behaviour. Carbonation could be of higher importance in dry environment, since CO_2 would better diffuse through the material's pore network [26]. Also, the formation of vaterite is encouraged in dry conditions [24].

Craeye et al. [27] studied the effect of gamma rays (^{60}Co) at 2.0 Gy/h and 7.8 Gy/h on cementitious samples during the hardening process with a total absorbed dose range of 0.042 kGy to 5.3 kGy. They found an overall strength reduction with increasing absorbed dose of gamma radiation. 75% of the tests resulted in a strength reduction of more than 5%. The maximal reduction was observed for samples which were cured for 24 h prior to irradiation to a total absorbed dose of 1.3 kGy. Ettringite needle formation [29] was observed in some cases. The formation of the expansive ettringite could cause internal microcracking within the mortar microstructure leading to a lower strength.

Radiation effects on hardened alkali-activated materials as alternatives for ordinary cementitious barriers have been studied by Lambertin et al. [22] using gamma rays from external ^{60}Co sources (600 Gy/h) up to 750 kGy. They found that gamma rays altered the microstructure of the studied materials due to the radiolytic hydrogen production. The same was observed by Chupin et al. [5]. An increase of the compressive strength by 10% was observed, probably because of a densification of the structure under gamma irradiation [22]. A decrease in the average Si-O-Al bonding angle due to gamma radiation was observed by Deng et al. [21]. According to Deng et al. [21] and Leay et al. [28] , gamma rays do not produce significant morphological changes, except for changes in the pore structure. All these studies were performed on hardened samples.

In this study the effect of gamma radiation is investigated on synthetic plasma slag (PS) based IPs using dose rates of 0.0016 kGy/h to 2 kGy/h and up to total absorbed doses of 0.032 kGy to 624 kGy]. The effect on microstructural properties and macromechanical behaviour is studied. Plasma slag is one of the materials streams produced when treating calorific waste using a plasma gasification reactor. The ashes produced during gasification are melted and cooled rapidly to form a vitrified phase [29]. This slag mainly consists of Si, Fe, Ca and Al oxides. Danthurebandara et al. [30] concluded that PS valorisation via IP production yields high environmental and economic benefits. The input products of Na_2SiO and NaOH mainly determine the beneficial impacts. However, the valorisation of PS as an IPs reduces CO_2 emission related to the production of OPC [31]. PS is more than 90% amorphous [32] when subjected to high cooling rates during solidification. This leads to a low water demand and easy dissolution of the precursor when in contact with (low molarity) alkaline solutions. A three phase system of binder, unreacted particles and voids is created.

2 Material and methods

2.1. Inorganic Polymer

A synthetic plasma slag was produced using urban solid waste incinerated bottom ash, iron ore, limestone and sand to create an ash with a similar composition to enhanced landfill mining ash as reported in Machiels et al. [29]. The melt was quenched using water jets and a water tank to obtain a vitrified material with limited crystalline phases (< 2 wt%). [29]

The quenched glass was crushed until a particle size lower than 5 mm after which further size reduction was performed using a ball mill until a Blaine value of $(4.07 \pm 0.04) \cdot 10^3$ cm²/g according to EN 196-6 was obtained [33]. The milled slag had a density of (3.094 ± 0.009) g/cm³ measured using a Quantachrome Multipycnometer MVP-6DC and a particle size distribution of D_{10}= (1.50 ± 0.06) µm, D_{50}= (10.2 ± 0.7) µm and D_{90}= (40 ± 2) µm. The chemical composition of the synthetic PS was determined using X-ray fluorescence analysis (Bruker S8 TIGER). High amounts of SiO_2, FeO, CaO and Al_2O_3 were detected, as can be observed in Table 1.

Table 1: Chemical composition of synthetic plasma slag (PS) and inorganic polymer (IP) according to XRF.
*expressed as Fe_2O_3

wt.%	SiO_2	FeO	CaO	Al_2O_3	MgO	TiO_2	K_2O	Na_2O	CuO	MnO
PS	29.4	27.9	26.8	13.4	0.8	0.7	0.6	0.2	0.1	0.1
IP	34.0	24.1*	21.1	11.9	0.9	0.5	0.5	6.3	0.1	0.1

The IP pastes were produced by mixing the dry milled slag with a sodium silicate activation solution in a solid to liquid ratio of 2.6 g/ml. The activation solution was characterised by a SiO_2/Na_2O molar ratio of 2.0 and a H_2O/Na_2O molar ratio of 29.0. The paste was cast in plastic cubic moulds of 25 mm³ and was manually tapped for 30 seconds to eliminate air bubbles. The samples were cured at a temperature of (28.8 ± 0.5) °C and a relative humidity of (54 ± 10) % for a further defined period before irradiation.

A dense microstructure as shown by scanning electron microscopy (SEM) in Figure 1 is obtained with a low BET value: (12 ± 2) m²/g measured on samples after 28 days hardening using TRISTAR 3000 Micromeritics with N_2 sorption measurements at -196.2 °C. According to Leay et al. this would be beneficial to a low H_2 yield from radiolysis [28].

2.2. Irradiation set-up

Samples were hardened for 1 hour, 24 hours or 28 days prior to irradiation. Table 2 shows the characteristics of the three types of gamma sources used in the irradiation tests (A-C).

Table 2: Three types of gamma emitting sources used for irradiation of IP samples.

	A **Low dose rate**	**B** **Intermediate dose rate**	**C** **High dose rate**
Source	^{60}Co	^{137}Cs	^{137}Cs
Energy	1.173 MeV, 1.332 MeV	0.662 MeV	0.662 MeV
Activity	2 TBq	35 TBq	123 TBq
Max dose rate	7.1 ± 0.7 Gy/h 1.6 ± 0.2 Gy/h	152 ± 8 Gy/h	2 kGy/h
Time before irradiation	24 h or 28 d	1 h	24 h

For the low dose irradiation test (A), two times 16 samples were placed at two different distances under the ^{60}Co-source. The dose rate determined by film dosimetry using a radiochromic film (Gafchromic EBT), calibrated using a ^{60}Co-source, was at the upper level equal to (7.1 ± 0.7) Gy/h and at the lower level equal to (1.6 ± 0.2) Gy/h. All samples were covered with an acrylic glass plate of 5 mm thick so that the maximum dose is received at the upper surface of the samples. The irradiated surface was limited to 50 mm from the central axis in order not the induce more than 5 % deviation from the average dose rates. 10 sets of samples (A1-A10) hardened for 24 hours or 28 days prior to irradiation (t_{prior}) were irradiated for a certain time interval t_{irr} between 24 hours and 100 days resulting in a received total dose range of 0.032 kGy to 16.8 kGy. Samples were characterised immediately after irradiation.

For intermediate dosing tests (B), a ^{137}Cs source (IBL 437 C irradiator) with a dose rate of (152 ± 8) Gy/h was used to irradiate 6 samples for 1 hour (t_{prior} = 1 h) after casting. The dose rate and dose distribution were analysed using EBT3 grafchromic films calibrated using a 6 MeV Linac, indicating no deviations in dose rate larger than 5 %. Since setting of the material only starts after 4.5 hours (NBN EN 196-3:2016) [34], no large amount of IP binder gel was formed when the irradiation was started. The samples were rotated in a cylindrical sleeve in order to prevent delivered dose inhomogeneities. Five irradiation periods t_{irr} were selected between 1 hour (0.152 kGy) and 26 days (95 kGy). After irradiation, samples (B1-B7) were stored in the curing chamber at (28.8 ± 0.5) °C and (54 ± 10) % relative humidity until 28 days of total hardening before characterisation.

The dose rate for the high dose rates experiments (C) was approximately 2 kGy/h. Only samples hardened for 24 hours (t_{prior}= 24 h) were irradiated for t_{irr} varying between 2.5 hours (5 kGy) and 13 days (624 kGy). Sample sets C1-C6 each composed of eight samples were characterised immediately.

For the characterisation techniques, a reference sample, identical to the others, was considered for each different irradiation test. Except for the irradiation, the same procedures were applied to these reference samples. The reference samples were kept at the same ambient conditions as the irradiation samples.

2.3. Evaluation of irradiation effects

2.3.1. Macro-mechanical behaviour

Compressive strengths tests were performed to evaluate the mechanical properties of the prismatic samples of (25 x 25 x 20) mm³. The tests were executed in triplicate. Uniaxial tests were performed according to NBN EN 12390-3 [35] using ZWICK Z050 with a compression speed of 1.0 mm/min. The maximum compressive strength (P_c) in MPa was calculated as the maximum load at fracture (F_c) in Newtons divided by the contact area of the auxiliary plates (A) in mm².

The relative strength change (D_f) illustrates the relative change in compressive strength of the irradiated samples ($P_{c\text{-}IRR}$) in respect to the compressive strength of the reference samples ($P_{c\text{-}REF}$).

2.3.2. Microstructural properties

Porosity measurements were performed using several techniques since no single technique can provide a full multiscale characterisation: Scanning Electron Microscopy (SEM), Water Absorption Test (WA-test) and Mercury Intrusion Porosimetry (MIP). Each technique delivers information on a different scale. For all techniques, oven dried (40 °C) samples were used.

(i) SEM was used to evaluate the microstructure in the macropore region (> 1 µm) using a Tabletop Microscope TM3000 (Hitachi, Krefeld, Germany) with an accelerating voltage of 15 kV. Samples were not polished or coated in order not to induce surface artefacts. A low vacuum was applied during SEM-analysis to avoid charging up effects without the need to apply a conductive coating layer. Unreacted particles and cracks were identified using a global threshold level for binarization of the grayscale images based on Otsu's method [36]. Noise from the images was filtered using a median filter and large shades were removed using a top-hat filtering. Otsu's method was then used to define a grayscale threshold based on the grayscale histogram of the SEM-image to maximize the inter-class variance of the black and white pixels. The method was adapted to the local-binarization method of Li. et al. [37] to detect the cracks more precisely. MATLAB morphological operations (fill, clean, erode, dilate, etc.) were used to optimize the segmented image.

(ii) WA-test was performed following the ASTM C642 [38] test method for density determination and void determination in the region of 1 nm to 100 mm [39]. Three samples (20x20x20) mm³ of the same batch were analysed.

(iii) MIP was performed using the Micromeritics Autopore IV 9510. Samples (5x5x5) mm³ were additionally dried for 48 hours at 30 °C at 1 µm Hg and next dried for 5 min at 25 °C and 10 µm Hg. The samples were tested in the range of 0.01 to 414 MPa. Reproducibility of the analysis was tested by measuring two samples from the same batch. An experimental difference of 0.5 % was noted for the porosity of the samples. MIP is applicable to quantify pores in the 3.6 nm to 100 µm region.

2.3.3. Other properties

Attenuated total reflectance Fourier-transformed infrared (ATR-FTIR) was performed using a Bruker Alpha-P with diamond crystal on milled powder samples of the IPs; 32 spectra per sample were acquired from 4000 cm^{-1} to 380 cm^{-1} at a resolution of 4 cm^{-1}. The reported spectra are the result of the average of 5 measurements on a homogenized powder made of four different samples.

Thermogravimetric analysis (TGA 550 - TA instruments) of the samples was carried out from 20 °C to 1000 °C with a heating rate of 10 °C/min in a nitrogen atmosphere. The mass was measured up to 10^{-6} g precision.

In the high dose rate experiment, also the sample mass change and sample volume change in time was evaluated. The mass was measured using a semi-analytic balance (0.01 g). The dimensions for the volume determination were measured using a calliper (0.01 mm).

3 Results and Discussion

3.1. Low dose rate experiment (A)

Samples were hardened for 24 hours or 28 days and irradiated using a ^{60}Co source. Irradiated samples and reference samples were both tested for uniaxial compressive strength. The results of the experiment (1.6 Gy/h and 7.1 Gy/h) are listed in Table 3. At low doses (< 3 kGy), the irradiated samples show an overall decrease in compressive strength, however no significant change was observed due to the large spread in the results. At higher doses (> 3 kGy), an increase of compressive strength is visible in most cases (samples A5.1, A4.2 and A5.2). Both the samples hardened for 24 hours and 28 days show this increase in strength, however only a significant increase could be observed for the samples A5.2, t_{prior} = 28 days. The reference samples had a compressive strength of (31 ± 2) MPa and the irradiated samples had a compressive strength of (36 ± 2) MPa. Notice that the time prior to irradiation also seems to affect the strength change of the material when irradiated.

Compared to literature, IPs have a better resistance to low dose rate gamma irradiation than OPC-based cements. 75 % of the self-compacting mortar samples tested by Craeye et al. [27] show a reduction in strength higher than 5%. Of the IPs tested, only 12 out of 30 samples (40 %) irradiated after 24 hours of hardening show a decrease in strength larger than 5%. For all samples A1-A5, the WA and MIP tests (results are not shown) revealed no significant irradiation effect on the porosity of the samples. Water content of the samples was determined by TGA analyses and no differences were present.

Table 3: Strength change relative to reference in low dose rate experiment (A) – t_{prior} = 24 h and 28 d – with one standard error of the mean. Samples Ax.1 are irradiated at <1.6 Gy/h and Ax.2 are irradiated at <7.1 Gy/h/.

ID	Dose rate (Gy/h)	t_{irr} (h)	Dose (kGy)	D_f (%) t_{prior} = 1d	D_f (%) t_{prior}=28 d
A1.1	1.57	20	0.032 ± 0.004	+6 ± 1	-
A2.1	1.57	46	0.072 ± 0.009	-4 ± 1	-13 ± 3
A3.1	1.56	671	1.0 ± 0.1	-20 ± 2	+ 2 ± 1
A4.1	1.54	1439	2.2 ± 0.2	-5 ± 2	-14 ± 2
A5.1	1.49	2400	3.6 ± 0.4	+5 ± 2	-
A1.2	7.06	20	0.14 ± 0.01	-9 ± 2	-
A2.2	7.05	46	0.32 ± 0.03	-22 ± 2	-15 ± 4
A3.2	7.01	671	4.7 ± 0.5	-1.8 ± 0.2	-7 ± 4
A4.2	6.90	1439	10 ± 1	(+6 ± 2) · 10^1	+9 ± 2
A5.2	6.71	2400	16 ± 2	+26 ± 8	+18 ± 1

Also, the SEM images (Figure 1) revealed no visible effect on the microstructure. In low dose rate experiment (A), almost all the samples showed a decrease in density of between 0.2% to 1.1%. However, no correlation was found between the decrease in compressive strength and the decrease in density.

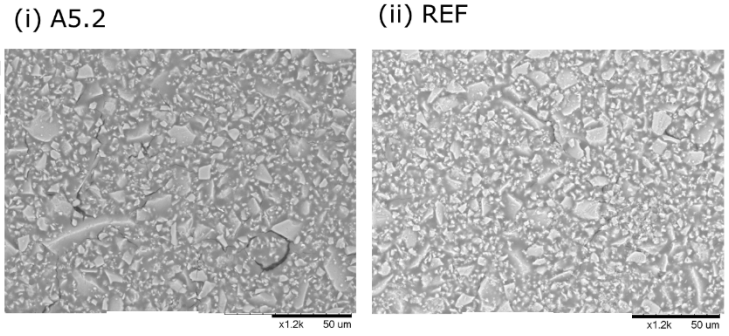

Figure 1: Scanning Electron Microscopy (SEM) images at 1200x of (i) irradiated samples (A5.2) and (ii) its reference sample - t_{prior} = 24 h. The light grey phases are unreacted slag particles and the dark grey phase is reacted IP binder.

3.2. Intermediate dose rate experiment (B)

Samples were hardened for 1 h and irradiated at a dose rate of 152 Gy/h using a ^{137}Cs source. An uniaxial compressive strength test on the irradiated and reference samples was performed. A significant decrease in compressive strength was found for the samples which received doses up to 3.6 kGy (B1-B3 in Figure 2). However, for the samples B4 and B5, which received doses higher than 3.6 kGy, an increased strength was observed. A 33% higher strength was measured for the samples with a dose of 95 kGy. An inversed trend was observed for porosity results of the WA-test (Figure 2). A higher porosity was measured for the irradiated samples with low doses (≤ 25 kGy) while a decrease of 22% was visible for the samples irradiated to 95 kGy (B5).

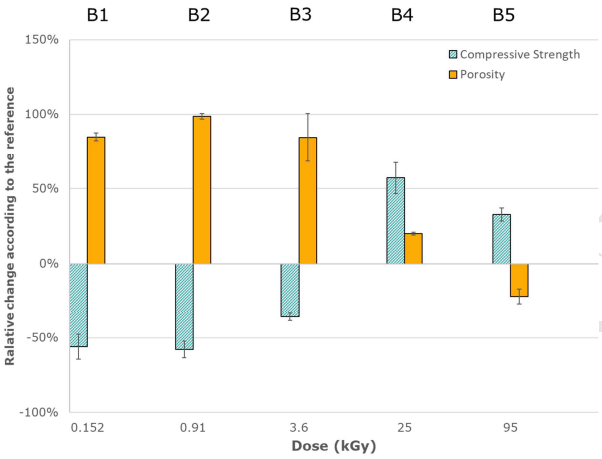

Figure 2: Relative change of compressive strength and relative change of porosity (WA-test) of irradiated samples compared to the reference samples – t_{prior} = 1 hour – with one standard error of mean.

The porosity and pore size distribution of B5 and reference samples were determined using MIP analysis. As shown in Figure 3, B5 has a higher level of pores below 10 nm with respect to the reference sample. Moreover, B5 has a significantly lower number of pores in the 10 to 100 nm region. The peak at 50 nm in the distribution curve of the reference sample is almost absent in the curve of B5. It can thus be stated that for samples only hardened for 1 hour prior to irradiation, a shift in pore size distribution occurs towards the smaller pore sizes. This causes the total porosity to decrease and the total pore area to increase. This could also explain the lower porosity of B5 from the WA-test and its higher strength. Since the sample is still liquid when the irradiation starts, porosity is easily affected due to e.g. shrinkage effects. The time of hardening of the sample prior to irradiation will thus highly influence the effect of gamma rays on the IP's microstructure. Also Lambertin et al. [22] observed a shift in pore size distribution, giving rise to two peaks in the pore size distribution for the irradiated samples instead of one peak for the reference samples. This phenomenon is explained as the reorganization of the thin pore walls [22].

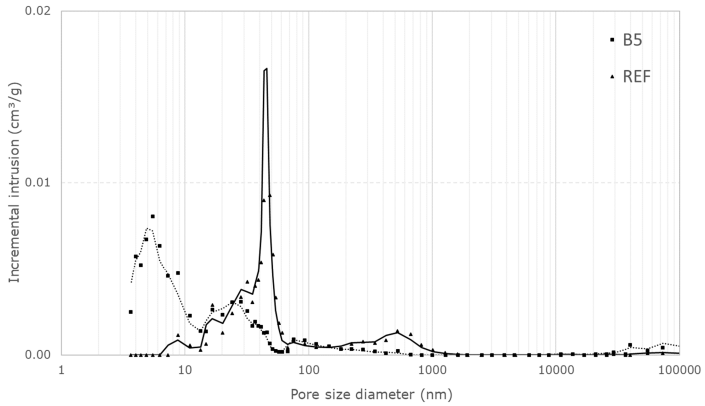

Figure 3: Pore size distribution of irradiated sample (B5) compared to a reference sample – t_{prior} = 1 h.

For the same two samples, a TGA analysis and ATR-FTIR analysis were performed. Both tests revealed a higher water content for sample B5 compared to the REF. TGA analysis indicated a water content of 16 wt% for sample B5 where the REF only has a water content of 8-9 wt%.

ATR-FTIR (Figure 4) confirms the higher water content of sample B5 with larger peaks present at the water bands at 3000 cm^{-1} to 3500 cm^{-1} and 1650 cm^{-1} to 1655 cm^{-1}. Moreover, a slightly larger peak is present from 800 cm^{-1} to 1000 cm^{-1} corresponding to Si-O(-T) stretching vibration (T = Al or Si). This may be attributed to a better tetrahedral network formed during the polymerisation reaction. Radiation induced polymerisation was also observed by Mubasher et al. [40]. Since this is a polycondensation reaction, this could also explain the higher free water content for B5. Moreover, more NASH gel may be formed thus leading to more hydrates. The radiation induced polymerisation might also explain the higher compressive strength for the samples. This statement however, needs further investigation. The smaller peaks at 1500 cm^{-1} and 860 cm^{-1} for the irradiated samples, indicate that less carbonates are formed. The larger peak at 400 cm^{-1} to 500 cm^{-1} can be attributed to aluminosilicate internal vibrations [41]. Also the SEM-images (Figure 5) show larger amount of binder phase in case of the irradiated samples (B5) relative to the non-irradiated samples. From the SEM-image it might look as B5 is more porous than its reference which is not in accordance with the porosity results (Figure 2), indicating that the voids and cracks found in the image are mainly external cracks and that porosity changes occur at the level below 1 µm so it cannot be observed with SEM.

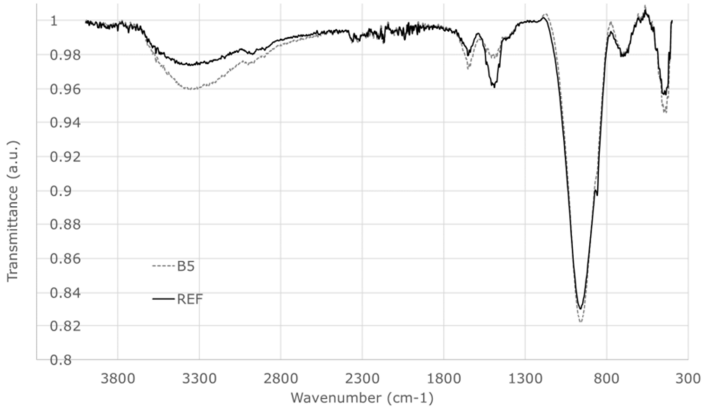

Figure 4: ATR-FTIR spectrum of irradiated sample (B5) compared to a reference sample - t_{prior} = 1 h.

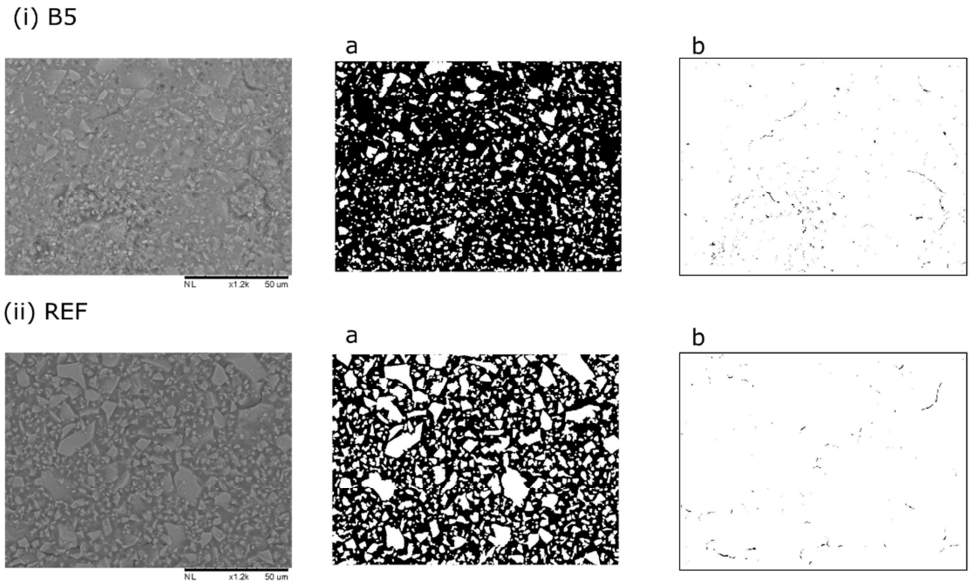

Figure 5: SEM images at 1200x of (i) irradiated sample (B5) and (ii) its reference sample – t_{prior} = 1 h. Each SEM image has been binarized first (a) to make the aggregates and binder better visible and second (b) to clearly visualise the cracks and voids.

3.3. High dose rate experiment (C)

Samples were hardened for 24 hours and irradiated at a dose rate of 2 kGy/h using a ^{137}Cs source. The uniaxial compressive strength was measured of the irradiated samples and the corresponding reference samples immediately after the irradiation was stopped. Figure 6 gives the trend for the relative change of compressive strength and the relative change of porosity in function of the total absorbed dose. No direct relationship could be found. The total absorbed dose varied between 4.7 kGy and 624 kGy. As shown in Figure 6, all the samples C1-C6 tested showed an increase in compressive strength. However, only a statistically significant increase is present for test C1, C2 and C4. The highest gain in compressive strength is registered for the C1, C2, C4 and C6-samples with an increase of 23 %, 16 %, 22 % and 15 % respectively. The reference samples of C1 had a compressive strength of (32 ± 3) MPa while the irradiated samples had a compressive strength of (39 ± 2) MPa at a dose of 4.7 kGy. For C2 there was an increase from (32 ± 3) MPa to (37 ± 1) MPa and for C4 from (27 ± 1) MPa to (33 ± 2) MPa. Radiation induced carbonation might be the cause of the increase in strength as reported by [17] for concrete. The increase of compressive strength up to 10% of hardened IPs under irradiation was already reported by Lambertin et al. [22] for a high dose delivered at a dose rate of 600 Gy/h under argon atmosphere and attributed to a densification of the matrix and a structural relaxation.

The same irradiation set-up as for this study was used by B. Craeye et al. [27] to evaluate the effect of gamma irradiation on self-compacting mortar. All the samples tested in Craeyes study showed a decrease in compressive strength, with a maximum decrease of 16.3 %. This indicates that IPs could be better resistant to gamma radiation than OPC mortars from mechanical point of view. However, the WA-test shows a relative increase in porosity for the IPs due to gamma irradiation.

An increase in porosity was observed for most of the samples tested (C1, C2, C4 and C5). The C1 samples showed the largest increase in porosity. The C1 reference samples had a porosity of (20.3 ± 0.2) % and the C1 irradiated samples had a porosity of (22.3 ± 0.2) %. For test C6 no significant increase is present. The increased porosity may be related to the accelerated drying (Table 5) due to radiolysis and gamma heating, which might also induce the formation of micro cracks and pores. However, the relative porosity change seems to decrease with increasing irradiation time. The formation of insoluble $CaCO_3$ in the pores and the further formation of IP binder (NASH-gel) can decrease the porosity in time. In the normal hardening process of an IP, water escapes from the matrix, creating a dryer environment which stimulates the formation of vaterite in a gamma radiation field. In wet conditions vaterite is easily transformed into stable calcite, a phenomenon which is not been observed for aragonite [42]. Vaterite, however, has a lower density than calcite and thus a higher pore filling efficiency [24]. Sample C6 is expected to have more carbonates than C1 due to the longer irradiation time. In addition, it is expected that more vaterite will be formed since the samples are dried during gamma radiation and due to the natural evaporation of water in the hardening process of the IP.

The increase in porosity was not confirmed by MIP-analysis (Figure 7). No significant changes were observed for the porosity of the samples within the range of 3.6 nm to 100 µm at high dose rate irradiation. This might be due to the formation of carbonates (e.g. Na_2CO_3) in the pores which can dissolve during the WA-test but do not dissolve in mercury when executing the MIP-analysis. In the pore size distribution however, very small changes are noticeable. For all the samples tested (1 sample for each irradiation of C1-C6) more pores were present for the irradiated samples in the 10 nm - 50 nm diameter region. Below 10 nm a small decrease in number of pores is visible. As shown in Figure 7 for C6, an increase of the number of pores in the 300-1000 nm diameter region is noticed. This can be explained by the pore wall reorganisation mechanism as mentioned by Lambertin et al. [22].

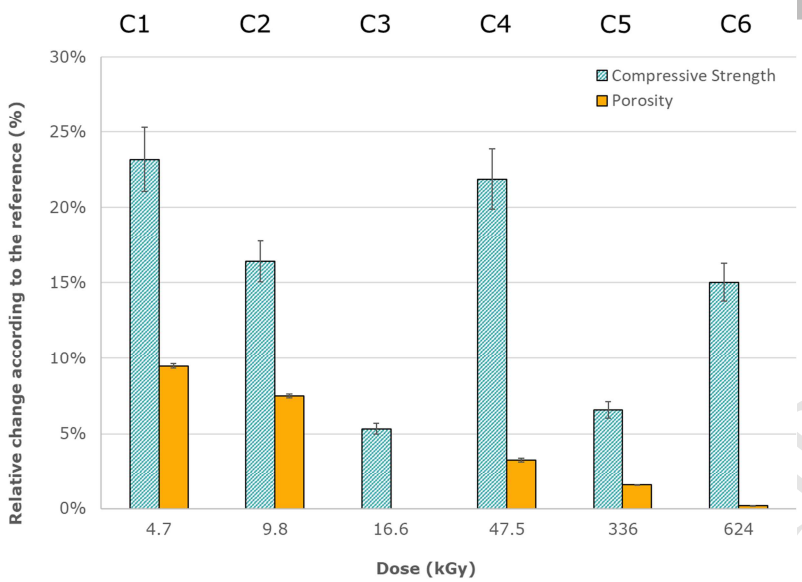

Figure 6: Relative change of compressive strength and relative change of porosity (WA-test) of irradiated samples compared to the reference samples – t_{prior} = 24 h – with one standard error of mean. The porosity result of C3 is not determined.

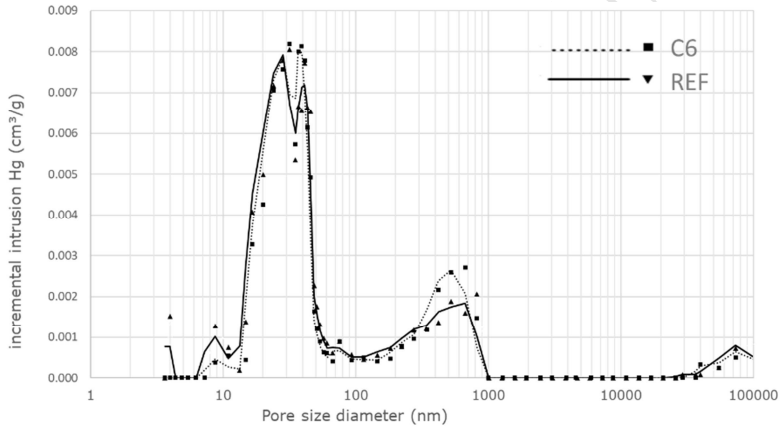

Figure 7: Pore size distribution of the irradiated sample C6 (624 kGy) compared to a reference sample - t_{prior} = 24 h.

A summary of SEM-images is given in Table 4. The images were binarized using a local-binarization method to visualise the cracks and voids. The SEM-images did not show morphological changes due to irradiation. Deng et al. [21] who irradiated fly ash based IPs up to 100 kGy using a 700 Gy/h ^{60}Co-source, could neither observe significant changes in the morphology.

The TGA results (Figure 8) clearly show a higher water content for the non-irradiated samples. However, the difference becomes smaller when the irradiation time becomes longer. In the beginning, gamma heating and hydrolysis cause an accelerated drying of the material. This process however diminishes when the samples cure since the free water content of the system decreases. Natural evaporation of water in the reference samples than causes the difference between the irradiated samples and reference samples to become smaller. For the irradiation of 24 hours (47.5 kGy), the difference in water content is the largest (3.17%). The first major decline in the TGA curves is attributed to the dewatering of free evaporable water and the interstitial water present in the sample and is located in the 20 °C - 250 °C region. The weight loss between 250 °C and 700 °C can be attributed to bound water present in the hydrates [43], [32]. As shown in Figure 8, the difference between the C samples and the reference samples is mainly from the free water and the interstitial water (20 °C – 250 °C). In addition, above 250 °C, samples C5 and C6 have a different behaviour with respect to the other samples. Where C1 – C4 lose most of their weight (95% of the total weight loss) from 20 °C - 250 °C, this is less (80%) for C5 and C6. The latter lose some extra mass in the 250 °C – 800 °C temperature range (Table 5). This effect is both present for the C samples and the reference samples and is the consequence of the further hardening with the formation of extra IP binder and the formation of carbonates in time. The mass loss from 400 °C -700 °C (Figure 8) is attributed to the decomposition of calcium carbonates [44], [45] or can be assigned to the decomposition of sodium carbonates. According to Thiery et al. [46] three modes of the

decomposition of $CaCO_3$ can be distinguished. The first and second modes are related to the crystalline polymorphs of $CaCO_3$. Mode I (780 °C – 990 °C) can be attributed to the most stable polymorph, calcite, mode II (680 °C – 780 °C) can be assigned to aragonite and vaterite, and mode III (550 °C – 680 °C) is associated with amorphous $CaCO_3$. Vaterite, which is the most unstable form can transform into calcite from a temperature of 356 °C [42], [47]. Aragonite, which is slightly more stable, starts to transform from 387 °C and will decompose at 615 °C [48]. However, these processes can take place over a wide temperature range of heating [48]. Moreover, the calcite produced according to an allotropic transformation is less stable and decomposes more likely within the temperature range of mode II due to impurities [46], [49]. Also particle size is important, as indicated by Salvador et al. who found that a larger particle size of $CaCO_3$ leads to a smaller activation energy [50].

It seems that more calcite decomposes for the reference samples and more amorphous $CaCO_3$ is present in the irradiated samples. When looking at the total mass loss for C5 and C6 in the region 250 °C - 800 °C, only a small difference is noticed between the irradiated and the reference samples: C5-IR loses 1.28 wt% while C5-REF loses 1.21 wt%. C6-IR loses 1.71 wt% and C6-REF 1.69 wt%. This could indicate that the different forms of $CaCO_3$ are present in different quantities or that different particles sizes of carbonates are present.

Table 4: Overview of SEM images at a magnification of 1200. Each SEM image has been binarized to make the cracks and voids in the material better visible – t_{prior} = 24 h.

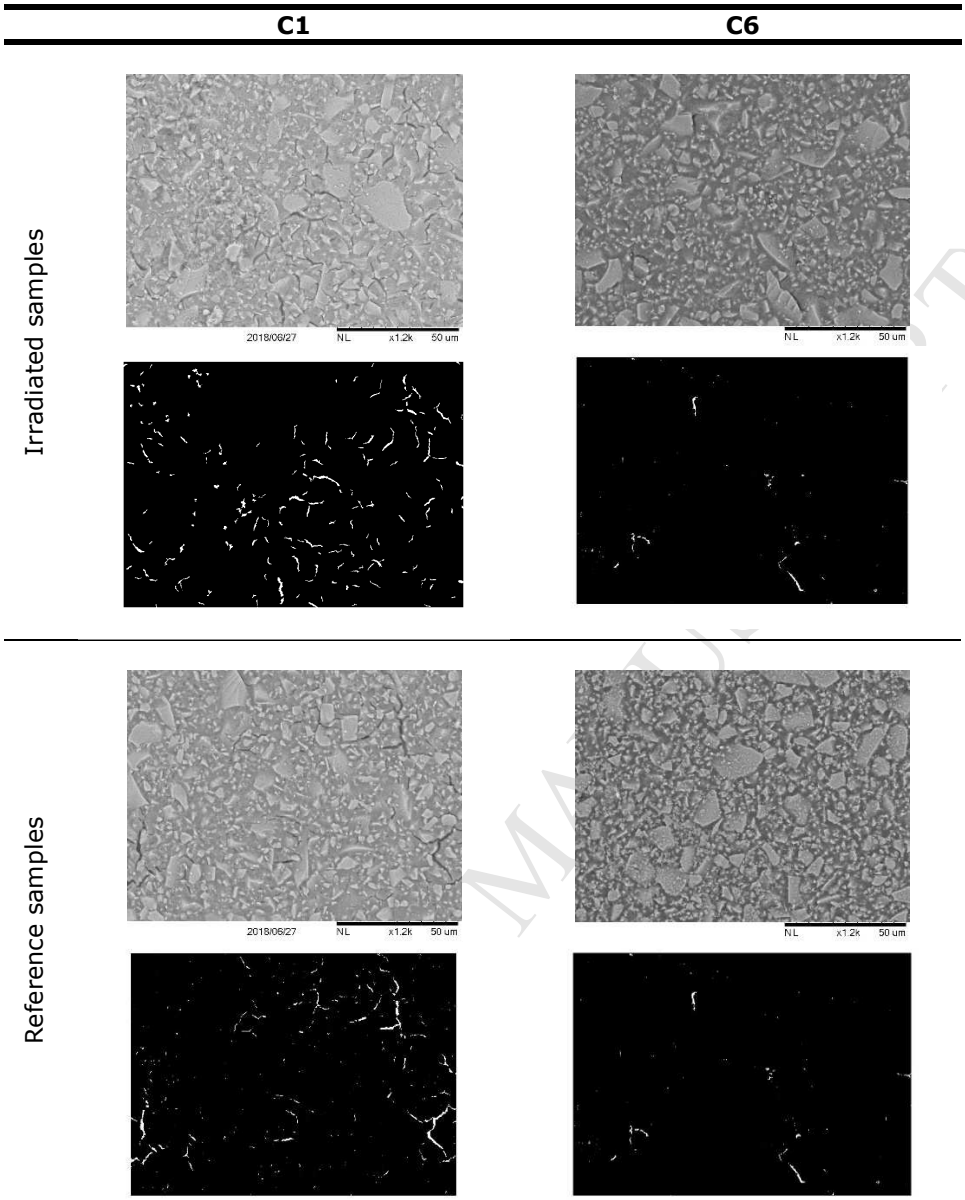

Table 5: TGA results recalculated to mass loss percentage of the original mass when heating the samples up to 800°C – t_{prior} = 24 h.

ID	Dose rate (kGy/h)	t_{irr} (h)	Dose (kGy)	Mass change IRs (wt%)		Mass change REFs (wt%)	
				20 – 250 °C	250 – 800 °C	20 – 250 °C	250 – 800 °C
C1	2	2.37	4.7	-10.36	-0.68	-12.90	-0.43
C2		4.92	9.8	-9.75	-0.48		
C3		8.33	16.6	-10.89	-0.40	-13.66	-0.44
C4		23.73	47.5	-6.62	-1.17	-9.68	-1.30
C5		168	336.0	-5.01	-1.28	-6.08	-1.21
C6		312	624.0	-5.50	-1.71	-6.54	-1.69

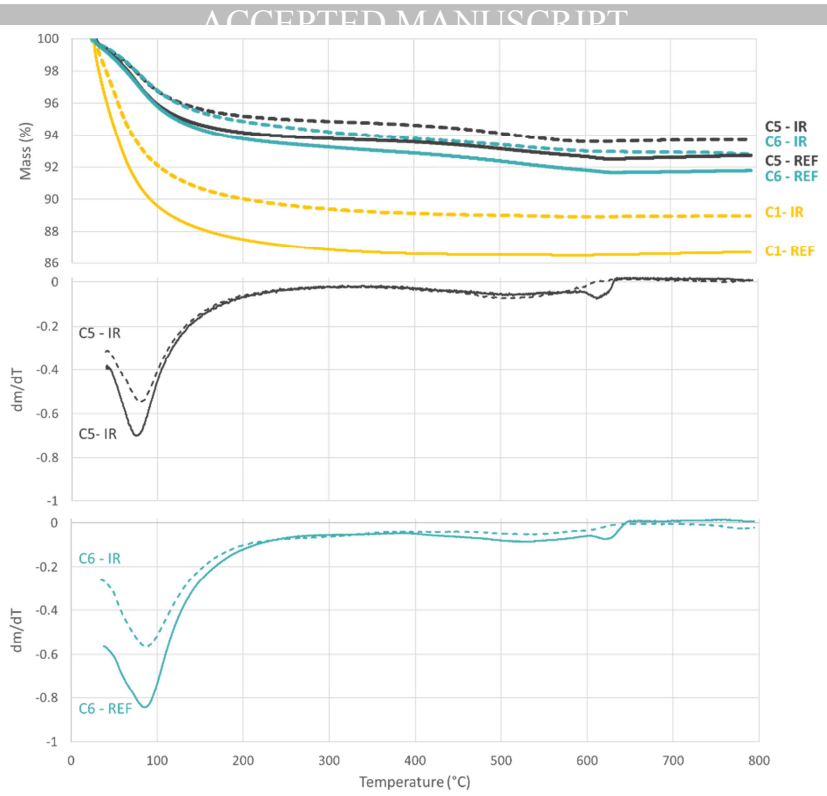

Figure 8: TGA curves and dm/dT curves of the C2 and C6 samples. For both tests (C2 and C6), a reference sample and an irradiated sample are plotted.

The higher water content at 2500 cm^{-1} to 3600 cm^{-1} for the reference samples and the difference in carbonates at 1250 cm^{-1} to 1560 cm^{-1} is also suggested by the infrared spectra. As an example, the infrared spectra of C6 are presented in Figure 9. The extra peak for the irradiated sample at 1404 cm^{-1} can be attributed to $CaCO_3$, indicating a radiation induced carbonation. Also at 860 cm^{-1} a small difference is present which is associated with the formation of $CaCO_3$. According to Sato et al. [25] peaks of vaterite are located at 1490, 1420, 1085, 870 and 750 cm^{-1}; peaks of aragonite at 1475, 1080, 855, 840 and 715 cm^{-1}; and peaks of calcite at 1430, 870, 845 and 715 cm^{-1}. This means that the peaks for samples C6 at Figure 9 are most likely linked to the formation of vaterite in the irradiated samples.

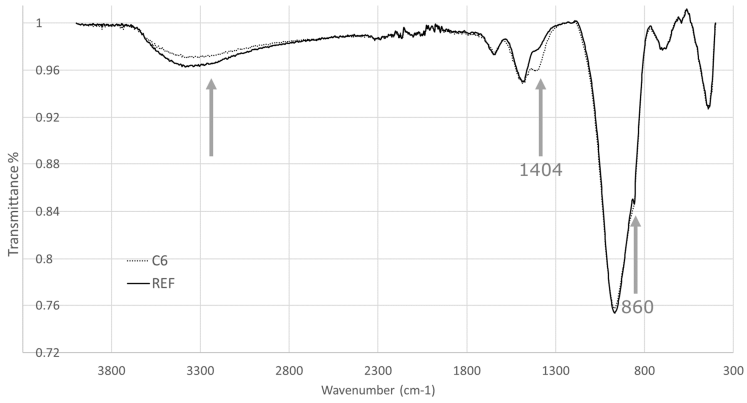

Figure 9: ATR-FTIR spectrum of irradiated samples (C6-IRs) compared to reference samples (C6-REFs) - t_{prior} = 24 h.

In the high dose rate experiment (C), the sample mass change and sample volume change in time was also evaluated. Each sample was measured before and after the irradiation. The relative change is expressed in Figure 10. As demonstrated, all the samples show a decrease in mass over time/dose, and a decrease in density. However, a plateau for both seems to be reached after 7 to 8 days of irradiation/hardening (C5) at a level of approximately -15% and -11% respectively. Also a decrease in volume is visible for both the irradiated and reference samples. It is clear that the irradiated samples have a higher mass and volume loss which is due to the accelerated loss of water as a result of radiolysis. However, the difference with the reference samples becomes smaller in time/dose. In most cases, except from C2, the irradiated samples have a lower density (approximately 12% after 7 to 8 days of irradiation) than the reference samples mainly attributed to a higher mass loss.

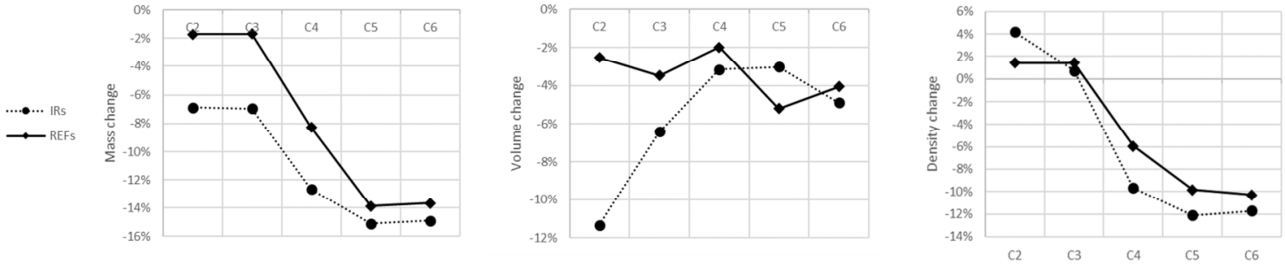

Figure 10: (i) Relative mass change (ii) relative Volume change and (iii) relative density change expressed as the relative difference of the samples measured before and after irradiation, t_{prior}= 24 h.

3.4. Overview and prospects

A graphical overview of the results from the compressive strength tests for all irradiation set ups is given in Figure 11. At low doses (< 5 kGy) no statistically significant change can be stated. Above 5 kGy however, a significant increase in compressive strength was found for all the samples. However, more irradiations exceeding the 5 kGy level are necessary, especially for the lowest dose rate of 1.6 Gy/h to support this conclusion. Also, it is not clear yet what will happen when the samples are irradiated to absorbed doses higher than the reference level of 2 x 10^5 kGy [24]. The relative change in strength seems to be more related to the total absorbed dose then to the applied dose rate. Moreover, the curing time prior to irradiation also affects the IP's response to gamma irradiation from the mechanical point of view. For the intermediate dose rate set-up at 152 Gy/h (B), the relative changes seem to be more pronounced then in the other set-ups, which might be related to the fact that the samples were in this case only hardened for 1 hour prior to irradiation. It is expected that in this case the radiation induced polymerization is of higher importance than the radiation induced carbonation.

We can compare the relative change in compressive strength of the samples of experiment A irradiated at 7.1 Gy/h with the samples of experiment C irradiated at 2 kGy/h since they are irradiated until the same dose rate. All the samples were hardened for only 24 h before irradiation. The mechanical response of the material to gamma irradiation seems to depend on the applied dose rate. For the samples of A.4.2 an increase of (+6 ± 2) · 10^1 % in strength was observed, while this was only (+16 ± 1) % for the samples in the C2 irradiation experiment.

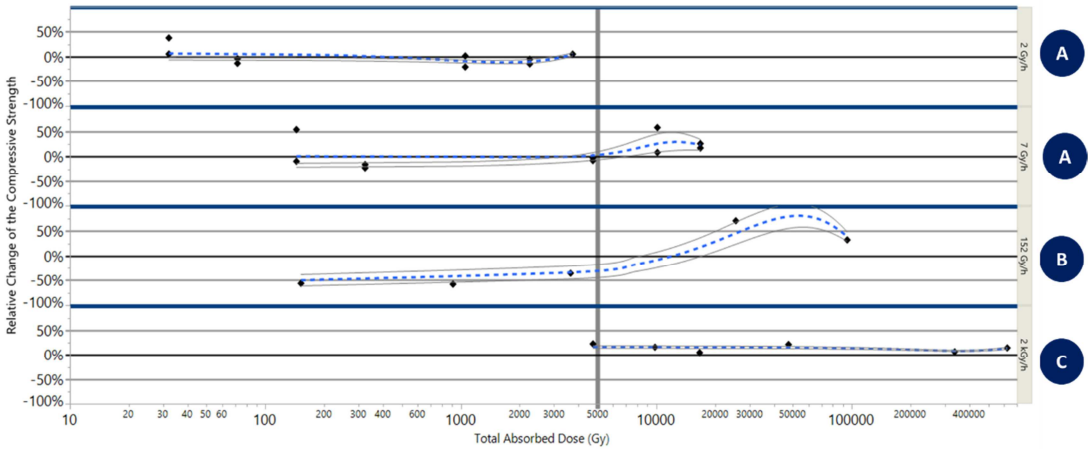

Figure 11: Relative change of compressive strength of the irradiated compared to the reference samples – in function of total absorbed dose (log scale) sorted per ascending dose rate with 80% confidence interval: A (1.6 Gy/h), t_{prior} = 24 h – A (7.1 Gy/h), t_{prior} = 24 h – B (152 Gy/h), t_{prior} = 1 h – C (2kGy/h), t_{prior} = 24 h.

The increase in strength can be related to the growth of carbonates e.g. $CaCO_3$ or Na_2CO_3 in the microcracks and pores [17], [24]. Next to radiation induced carbonation strengthening, a possible explanation for the strength increase could be the iron reduction under gamma radiation. The minimal amount of Fe^{3+} present in the Fe-rich precursor material and the additional amount of Fe^{3+} formed simultaneously with the polymerization reaction in the IP synthesis reaction [51]–[55] can be reduced in alkaline environment under gamma radiation [56], [57]. Due to gamma irradiation, a reducing environment is generated [23]. Under these conditions, non-structural Fe^{3+} from the initial dissolution step in IP formation can reduce to Fe^{2+}.Tetrahedral Fe^{3+} can be incorporated in an IP framework [52], [54], Fe^{2+} on the other hand will form two dimensional trioctahedral layers similar to $Fe(OH)_2$ which might contribute to a higher strength. Whether the reduction of Fe^{3+} to Fe^{2+} in the IP contributes to the strength increase of the IPs under gamma irradiation will be further investigated in future research.

The IPs tested show a better resistance to gamma radiation from a mechanical point of view compared to the mortar samples from Craeye et al. [27]. An increase of compressive strength of 10% was also observed by Lambertin et al. [22] for hardened metakaolin based sodium geopolymers which is comparable to the IPs used in this study.

4 Conclusions

Inorganic polymers based on plasma slag were ~~are~~ found to have a better gamma irradiation resistance from a mechanical point of view compared to OPC-based–samples. The IP samples irradiated to doses between 5 kGy and 624 kGy all show an increase in compressive strength compared to the non-irradiated samples. The IPs studied show a different behaviour when irradiated immediately after casting (B) or after 24 hours of hardening (A & C). IP samples irradiated immediately after casting show a higher increase in porosity and a clear shift in pore size distribution in favour of the smaller pores. The increase in strength in experiment B could be explained by a radiation induced polymerization reaction and a change in porosity. For all the samples irradiated, the increase in strength could be explained by the formation of amorphous carbonates and the reduction of iron.

Data availability

The raw/processed data required to reproduce these findings cannot be shared at this time as the data also forms part of an ongoing study.

Acknowledgements

The authors gratefully thank ing. Burak Yalvac from NuTeC UHasselt for the help with the dosimetrical analysis of the irradiation sources. The authors also express their appreciation to dr. ing. Krzystof Kierzek and from Wroclaw University of Science and Technology to perform the MIP-analysis. The authors also thank L. Arnout and L. Machiels from KU Leuven from providing the synthetic plasma slag. This study was supported by the Special Research Fund (BOF) of Hasselt University.

References

[1] J. Koťátková, J. Zatloukal, P. Reiterman, and K. Kolář, "Concrete and cement composites used for radioactive waste deposition," *J. Environ. Radioact.*, vol. 178–179, pp. 147–155, 2017.

[2] International Atomic Energy Agency, "The Behaviours of Cementitious Materials in Long Term Storage and Disposal of Radioactive Waste : Results of a Coordinated Research Project.," Vienna, 2013.

[3] J. L. Provis, "Geopolymers and other alkali activated materials: why, how, and what?," *Mater. Struct.*, vol. 47, no. 1–2, pp. 11–25, 2014.

[4] J. G. S. van Jaarsveld, J. S. J. Van Deventer, and L. Lorenzen, "Potential use of geopolymeric materials to immobilize toxic metals: Part I. Theory and applications," *Miner. Eng.*, vol. 10, no. 7, pp. 659–669, 1997.

[5] F. Chupin, A. Dannoux-papin, Y. N. Ravache, and J.-B. D'Espinose de Lacaillerie, "Water content and porosity effect on hydrogen radiolytic yields of geopolymers," *J. Nucl. Mater.*, vol. 494, pp. 138–146, 2017.

[6] J. Davidovits, *Geopolymer, Green Chemistry and Sustainable Development Solutions Chimie Verte et Solutions*. Saint-Quentin: Institut Géopolymère, 2005.

[7] N. Vandevenne *et al.*, "Incorporating Cs and Sr into blast furnace slag inorganic polymers and their effect on matrix properties," *J. Nucl. Mater.*, vol. 503, pp. 1–12, 2018.

[8] P. Duan, C. Yan, W. Zhou, W. Luo, and C. Shen, "An investigation of the microstructure and durability of a fluidized bed fly ash–metakaolin geopolymer after heat and acid exposure," *Mater. Des.*, vol. 74, pp. 125–137, 2015.

[9] P. Lichvar, M. Rozloznik, and S. Sekely, "BEHAVIOUR OF ALUMINOSILICATE INORGANIC MATRIX SIAL DURING AND AFTER SOLIDIFICATION OF RADIOACTIVE SLUDGE AND RADIOACTIVE SPENT RESINS AND THEIR MIXTURES," 2013.

[10] D. Majersky, S. Sekely, D. Zavodska, and M. Breza, "Application of Inorganic SIAL Matrix and Movable Technology in Solidification of the TRU Sludges and Sludge / Resin Mixtures," in *WM'06 Conference*, 2006.

[11] Z. Drace and M. I. Ojovan, "Cementitious materials for radioactive waste management within IAEA Coordinated Research Project," in *Proceedings of the International Conference on Radioactive Waste Management and Environmental Remediation, ICEM*, 2011, pp. 5–13.

[12] B. Florence, C. Cau-dit-Coumes, F. Frizon, and S. Lorente, Eds., *Cement-Based Materials for Nuclear Waste Storage*. Springer, 2013.

[13] H. K. Hilsdorf, J. Kropp, and H. J. Koch, "The Effects of Nuclear Radiation on the Mechanical Properties of Concrete," *Am. Concr. Inst.*, vol. 55, pp. 223–254, 1978.

[14] T. Ichikawa and H. Koizumi, "Possibility of Radiation-Induced Degradation of Concrete by Alkali-Silica Reaction of Aggregates," *J. Nucl. Sci. Technol.*, vol. 39, no. 8, pp. 880–884, 2012.

[15] P. Soo and L. Milian, "The effect of gamma radiation on the strength of Portland cement mortars," *J. Mater. Sci. Lett.*, vol. 20, no. 14, pp. 1345–1348, 2001.

[16] F. Vodák, V. Vydra, K. Trtík, and O. Kapičková, "Effect of gamma irradiation on properties of hardened cement paste - correct," *Mater. Struct.*, vol. 44, no. 1, pp. 101–107, 2010.

[17] T. M. Rosseel *et al.*, "Review of the Current State of Knowledge on the Effects of Radiation on Concrete," *J. Adv. Concr. Technol.*, vol. 14, no. 7, pp. 368–383, 2016.

[18] O. Kontani, S. Sawada, I. Maruyama, M. Takizawa, and O. Sato, "Evaluation of Irradiation Effects on Concrete Structure: Gamma-Ray Irradiation Tests on Cement Paste," in *Proceedings of the ASME 2013 Power Conference POWER2013*, 2013.

[19] A. Łowińska-Kluge and P. Piszora, "Effect of gamma irradiation on cement composites observed with XRD and SEM methods in the range of radiation dose 0-1409 MGy," *Natl. Meet. Synchrotron Radiat. Users*, vol. 114, no. 2, pp. 399–411, 2008.

[20] B. Hilloulin, M. Robira, and A. Loukili, "Coupling statistical indentation and microscopy to evaluate micromechanical properties of materials : Application to viscoelastic behavior of irradiated mortars," *Cem. Concr. Compos.*, vol. 94, pp. 153–165, 2018.

[21] N. Deng *et al.*, "Effects of gamma-ray irradiation on leaching of simulated 133Cs+ radionuclides from geopolymer wasteforms," *J. Nucl. Mater.*, vol. 459, pp. 270–275, 2015.

[22] D. Lambertin, C. Boher, A. Dannoux-Papin, K. Galliez, A. Rooses, and F. Frizon, "Influence of gamma ray irradiation on metakaolin based sodium geopolymer," *J. Nucl. Mater.*, vol. 443, no. 1–3, pp. 311–315, 2013.

[23] P. Bouniol and A. Aspart, "Disappearance of oxygen in concrete under irradiation: The role of peroxides in radiolysis," *Cem. Concr. Res.*, vol. 28, no. 11, pp. 1669–1681, 1998.

[24] I. Maruyama *et al.*, "Impact of gamma-ray irradiation on hardened white Portland cement pastes exposed to atmosphere," *Cem. Concr. Res.*, vol. 108, no. March, pp. 59–71, 2018.

[25] I. Maruyama, O. Kontani, A. Ishizawa, M. Takizawa, and O. Sato, "Development of System for Evaluating Concrete Strength Deterioration Due to Radiation and Resultant Heat - Prepared for International Atomic Energy Agency (IAEA) - IAEA-CN-194," 2012.

[26] D. L. Fillmore, "Literature Review of the Effects of Radiation and Temperature on the Aging of Concrete - Prepared for the Central Research Institute of Electric Power Institute - INEEL/EXT-04-02319," Idaho National Engineering and Environmental Laboratory, Idaho, 2004.

[27] B. Craeye, G. De Schutter, C. Vuye, and I. Gerardy, "Cement-waste interactions: Hardening self-compacting mortar exposed to gamma radiation," *Prog. Nucl. Energy*, vol. 83, pp. 212–219, 2015.

[28] L. Leay, A. Potts, and T. Donoclift, "Geopolymers from fly ash and their gamma irradiation," *Mater. Lett.*, vol. 227, pp. 240–242, 2018.

[29] L. Machiels, L. Arnout, P. Yan, and P. Tom, "Transforming Enhanced Landfill Mining Derived Gasification / Vitrification Glass into Low-Carbon Inorganic Polymer Binders and Building Products," *J. Sustain. Metall.*, vol. 3, no. 2, pp. 405–415, 2017.

[30] M. Danthurebandara, S. Van Passel, L. Machiels, and K. Van Acker, "Valorization of thermal treatment residues in Enhanced Landfill Mining: Environmental and economic evaluation," *J. Clean. Prod.*, vol. 99, pp. 275–285, 2015.

[31] J. L. Provis and J. S.J. van Denveter, Eds., *Geopolymers: structure, processing, properties and industrial applications*, 1st ed. Cambridge: Woodhead Publishing Limited, 2009.

[32] L. Kriskova, L. Machiels, and Y. Pontikes, "Inorganic Polymers from a Plasma Convertor Slag : Effect of Activating Solution on Microstructure and Properties," *J. Sustain. Met.*, vol. 1, no. 3, pp. 240–251, 2015.

[33] European Comittee for standardization, "EN 196-6:2010 - Methods of testing cement - Part 6: Determination of fineness," pp. 1–18, 2010.

[34] Bureau voor Normalisatie, "NBN EN 196-3:2016-Methods of testing cement - Part 3: Determination of setting times and soundness," Brussel, 2016.

[35] Bureau voor Normalisatie, "NBN EN 12390-3 - Testing hardened concrete - Part 3: Compressive strength of test specimens," 2nd ed., 2009.

[36] N. Otsu, "A Threshold Selection Method from Gray-Level Histograms," *IEEE Trans. SYSTREMS, MAN, Cybern.*, vol. 9, no. 1, pp. 62–66, 1979.

[37] L. Li, Q. Wang, G. Zhang, L. Shi, J. Dong, and P. Jia, "A method of detecting the cracks of concrete undergo high-temperature," *Constr. Build. Mater.*, vol. 162, pp. 345–358, 2018.

[38] ASTM International, "C 642: Standard Test Method for Density , Absorption , and Voids in Hardened Concrete 1," *1997*.

[39] L. M. Anovitz and D. R. Cole, "Characterization and Analysis of Porosity and Pore Structures," *Rev. Mineral. Geochemistry*, vol. 80, no. 1, pp. 61–164, 2015.

[40] T. A. Mubasher, L. Leay, M. Hayes, and E. Butcher, "Evaluation of Novel Geopolymer-based Materials for Nuclear Waste Treatment," in *NUWCEM - 3rd International Symposium on Cement-Based Materials for Nuclear Wastes*, 2018, pp. 1–5.

[41] A. Peys, L. Arnout, T. Hertel, and R. I. Iacobescu, "The Use of ATR-FTIR spectroscopy in the analysis of iron-silicate inorganic polymers," in *5th International Slag Valorisation Symposium*, 2017.

[42] M. Maciejewski, H. R. Oswald, and A. Reller, "Thermal transformations of vaterite and calcite,"

Thermochim. Acta, vol. 234, pp. 315–328, 1994.

[43] C. A. Rosas-Casarez *et al.*, "Experimental study of XRD, FTIR and TGA techniques in geopolymeric materials," *Int. J. Adv. Comput. Sci. Its Appl.*, vol. 4, no. 4, p. 25–30., 2014.

[44] S. A. Bernal *et al.*, "Gel nanostructure in alkali-activated binders based on slag and fly ash, and effects of accelerated carbonation," *Cem. Concr. Res.*, vol. 53, pp. 127–144, 2013.

[45] A. R. Sakulich, "Characterization of Environmentally-Friendly Alkali Activated Slag Cements and Ancient Building Materials - unpublished thesis," Drexel University, 2009.

[46] M. Thiery, G. Villain, P. Dangla, and G. Platret, "Investigation of the carbonation front shape on cementitious materials: Effects of the chemical kinetics," *Cem. Concr. Res.*, vol. 37, no. 7, pp. 1047–1058, 2007.

[47] F. Baitalow, G. Wolf, and M. G. Schmidt, "Thermochemical Investigations of Calcium Carbonate Phase Transitions," *J. Therm. Anal.*, vol. 52, pp. 5–16, 1998.

[48] G. T. Faust, "Thermal Analysis Studies on Carbonates, I-Aragonite and Calcite.," *Am. Mineral.*, vol. 35, pp. 207–224, 1950.

[49] C. Rodriguez-Navarro, E. Ruiz-Agudo, A. Luque, A. B. Rodriguez-Navarro, and M. Ortega-Huertas, "Thermal decomposition of calcite: Mechanisms of formation and textural evolution of CaO nanocrystals," *Am. Mineral.*, vol. 94, no. 4, pp. 578–593, 2009.

[50] A. R. Salvador, E. G. Calvo, and C. B. Aparicio, "Effects of Sample weight, particle size, purge gas and crystalline structure on the observed kinetic parameters of calcium carbonate decomposition.," *Thermochim. Acta*, vol. 143, pp. 339–345, 1989.

[51] S. Onisei, A. P. Douvalis, A. Malfliet, A. Peys, and Y. Pontikes, "Inorganic polymers made of fayalite slag : On the microstructure and behavior of Fe," *J. Am. Ceram. Soc.*, vol. 101, no. 6, pp. 2245–2257, 2018.

[52] S. Simon, G. J. G. Gluth, D. Banerjee, and Y. Pontikes, "The fate of iron during the alkali-activation of synthetic (CaO-) FeO x -SiO2 slags : An Fe K-edge XANES study," *J. Am. Ceram. Soc.*, vol. 101, no. 5, pp. 2107–2118, 2018.

[53] A. Peys, C. E. White, D. Olds, H. Rahier, B. Blanpain, and Y. Pontikes, "Molecular structure of CaO – FeOx – SiO2 glassy slags and resultant inorganic polymer binders," *J. Am. Ceram. Soc.*, vol. 101, no. 12, pp. 5846–5857, 2018.

[54] A. Peys, C. E. White, H. Rahier, B. Blanpain, and Y. Pontikes, "Alkali-activation of CaO-FeOx-SiO2 slag: Formation mechanism from in-situ X-ray total scattering," In Publication.

[55] A. Peys, A. P. Douvalis, V. Hallet, H. Rahier, B. Blanpain, and Y. Pontikes, "Inorganic polymers from CaO-FeOx-SiO2 slag: the start of oxidation of Fe and the formation of a mixed valence binder," In Publication.

[56] M. Azmi, A. Hamid, and N. Kamil, "pH-dependent magnetic phase transition of iron oxide nanoparticles synthesized by gamma-radiation reduction method," *J Radioanal Nucl Chem*, vol. 301, no. 2, pp. 399–407, 2014.

[57] E. B. Gracien, Z. Ruimin, X. Lihui, L. K. Kanza, and I. Lopaka, "Effects of pH on the morphology of iron oxides synthesized under gamma-irradiation," *J. Radioanal. Nucl. Chem.*, vol. 270, no. 2, pp. 473–478, 2006.